Process Safety and Environmental Protection 210 (2026) 108730

Contents lists available at ScienceDirect

Process Safety and Environmental Protection

journal homepage: www.journals.elsevier.com/process-safety-and-environmental-protection

Post-venting immersion cooling of over-heated battery: Effect of thermal runaway risk, cell scale, and quenching strategy

Lei Zhang [a,b], Feiyu Guan [a], Yichao Zhang [a], Yuying Chen [a], Yanhui Liu [a], Congliang Ye [a], Shi Liu [c], Xinyan Huang [a,b,*]

[a] Department of Building Environment and Energy Engineering, The Hong Kong Polytechnic University, Hong Kong
[b] Research Institute for Smart Energy, The Hong Kong Polytechnic University, Hong Kong
[c] National Institute of Guangdong Advanced Energy Storage, Guangzhou, China

ARTICLE INFO

Keywords:
Battery safety
Thermal runaway prevention
Emergency cooling
Safe venting mode
Battery fire suppression
Energy density

ABSTRACT

The risk of thermal runaway, fire, and explosion remains the ultimate barrier to battery systems. The costly immersion cooling offers a good thermal management solution, but it still cannot quench the battery thermal runaway. This study explores the emergency immersion cooling of a battery by dielectric fluid (HFE-7200) in the time window between venting and thermal runaway for 13 types of cylindrical cells, ranging from 18650 to 32650 and from 447 to 1190 Wh/L. Three post-venting modes are observed: (I) internal meltdown with a high risk of thermal runaway, (II) lid open during venting with a low risk of thermal runaway, and (III) safe venting without risk of thermal runaway. We found that larger cells undergoing safe venting or lid open require no more than 1/16 of the cell volume of dielectric coolant to completely eliminate thermal-runaway risk. The high-power smaller cells, exhibiting internal meltdown, reach peak temperatures over 600 °C during thermal runaway, requiring up to 1/2 of the cell volume of coolant to prevent the onset of thermal runaway. Heat transfer analysis is proposed to reveal the minimum coolant-to-cell volume ratio for post-venting immersion cooling of a battery with different volumes, specific surface areas, and energy densities. This study further verifies the early emergency cooling strategy for preventing battery thermal runaway and explores its scale effect for larger batteries, guiding the design of future battery safety management systems.

1. Introduction

Lithium-ion batteries (LIBs) have revolutionized modern energy storage, powering everything from portable electronics to electric vehicles and grid systems due to their unparalleled energy density and efficiency (Fan et al., 2026; Nasiri and Hadim, 2024). However, the relentless drive toward higher energy density and larger cell formats has introduced severe safety challenges (Cheng et al., 2025; Huang et al., 2025; Liu et al., 2026a; Wang et al., 2022), most notably thermal runaway and consequent fire and explosion events (Chen et al., 2025; Liu et al., 2025). For example, a serious fire and explosion occurred at the Beijing Dahongmen Battery Energy Storage Station in 2021, resulting in three deaths (including two firefighters) (Hu et al., 2025). Felicity Ace, a 60,000-tonne roll-on/roll-off cargo ship, caught fire due to battery thermal runaway in electric vehicles in the middle of Altanic Ocean and eventually sank with about 4000 luxury cars in 2022. In battery pack environments, thermal runaway triggered by external heating poses a systemic threat: the heat released from a single failing cell can rapidly destabilize its neighbors, triggering a catastrophic cascading failure across the entire module without effective process safety management and emergency response. (Mao et al., 2025; Ouyang et al., 2025; Wang et al., 2024; Zhang et al., 2025a). Thus, the development of effective thermal management strategies capable of severing this propagation chain is not merely an engineering improvement, but a fundamental prerequisite for the safety of next-generation high-energy battery packs (Sarkar et al., 2024; Shabana et al., 2025).

Significant efforts have been devoted to developing robust thermal management and process safety control strategies to mitigate battery hazards (Liu et al., 2026b). Conventional approaches can be broadly categorized into fire suppression agents and external cooling methods (Liu et al., 2023; L. Zhang et al., 2024). Fire suppression media, such as water mist (Liu et al., 2020; Wang et al., 2025), heptafluoropropane (Liu et al., 2024), and dodecafluoro-2-methylpentan-3-one (Zhang et al., 2023), are widely used to extinguish open flames and reduce toxic emissions. However, their primary limitation lies in their insufficient

* Corresponding author at: Department of Building Environment and Energy Engineering, The Hong Kong Polytechnic University, Hong Kong.
E-mail address: xy.huang@polyu.edu.hk (X. Huang).

https://doi.org/10.1016/j.psep.2026.108730
Received 30 January 2026; Received in revised form 1 March 2026; Accepted 12 March 2026
Available online 14 March 2026

Nomenclature

LIB	Lithium-ion battery
SOC	State of charge
SSA	Specific surface area, 1/m
TR	Thermal runaway

Symbols

A	Surface area of cell, m^2
c_p	Specific heat capacity, J/kg/K
D	Diameter of the cell, m
E	Energy, kJ or Wh
H	Latent heat of vaporization, J/kg
h	Heat transfer coefficient, $W/m^2/K$
m	Mass, kg
$\dot{Q}$	Heat generation rate, W
T	Temperature, ℃
V	Volume, m^3

Greeks

Φ	Coolant to cell volume ratio, (-)
ε	Energy density, Wh/L

Subscript

a	Ambient
B	Battery
$boil$	Boiling
c	Coolant
min	Minimum
$diss$	Dissipation
eff	Effective
gen	Generation
max	Maximum
$surf$	Surface of the battery

cooling capacity; while effective at suppressing visible fire, they often fail to arrest the self-heating reactions, leading to high risks of reignition. On the other hand, traditional thermal management systems (Zhang et al., 2022), such as air cooling (Ahmad et al., 2023; Zhao et al., 2021), liquid cold plates (Wang et al., 2025; Zhang et al., 2024) and heat pipes (Su et al., 2025; Weragoda et al., 2023), rely on indirect heat exchange through the cell surface or module casing. These methods suffer from high thermal resistance and are often too slow to dissipate the rapid heat generation once thermal runaway has initiated. Although more aggressive measures like liquid nitrogen injection (Ping et al., 2024) have been explored for rapid cooling, they pose challenges regarding system complexity and potential thermal shock. Consequently, existing methods struggle to penetrate the battery pack to directly quench the cell core after venting, highlighting the critical need for a more effective emergency cooling strategy like immersion cooling (Liang et al., 2026; Liu et al., 2023).

Immersion cooling, where cells are directly submerged in a dielectric fluid, has been widely applied for battery thermal management (Ahmad et al., 2024; Feng et al., 2018; Liu et al., 2023; Wahab et al., 2025). In terms of cooling performance, immersion cooling can be better than conventional thermal management strategies (Roe et al., 2022; Xin et al., 2025), such as forced-air cooling (Yu et al., 2025) and liquid cold plates (Fang et al., 2025). With the additional phase-change latent heat via nucleate boiling, as shown in Fig. 1(a), immersion cooling achieves heat flux dissipation rates orders of magnitude higher than traditional single-phase methods (Birbarah et al., 2020; Liang et al., 2026; Roe et al., 2022). However, the existing immersion cooling strategies are designed either for battery thermal management before the occurrence of venting and thermal runaway, which is not designed as a battery fire suppression system. Meanwhile, after the occurrence of thermal runaway, the immersion of the entire battery into coolant still cannot stop the thermal runaway, because it is too late and the cooling is insufficient (Liang et al., 2026).

Previously, we found there could be a time window of 1–5 min between battery venting and thermal runaway for the 18650 cell (Zhang et al., 2025b). During this critical time window, a small amount of immersion coolant of water, HFE- 7200, silicone oil, and transformer oil (about 1 mL with a coolant-cell volume ratio < 1/16) can effectively suppress the battery post-venting self-heating and prevent the onset of thermal runaway, as illustrated in Fig. 1(b). However, every lithium-ion battery is different in size, shape, energy density, and the design of the safety valve, so it is important not to overlook the profound scale effect

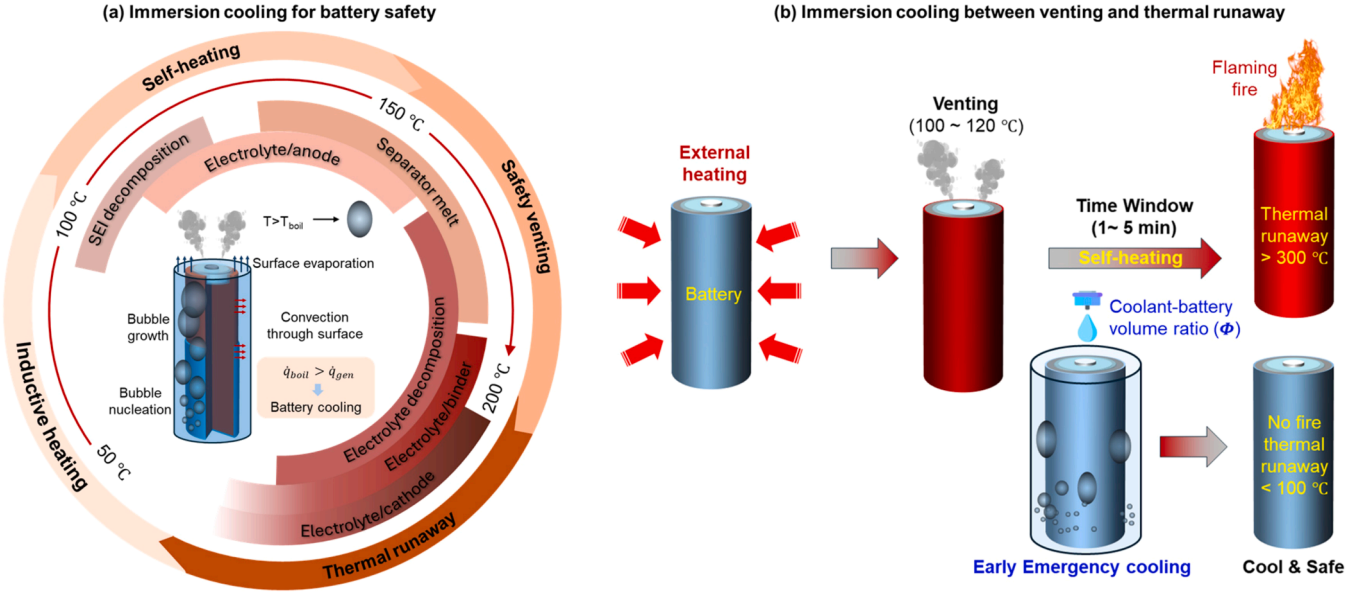

Fig. 1. Schematic illustration of (a) immersion cooling for battery safety, and (b) immersion cooling between venting and thermal runaway (Zhang et al., 2025b).

of the battery cell (Chen et al., 2025; He et al., 2024; Liu et al., 2024). Systematic cross-scale comparisons are notably absent in their venting and thermal-runaway behaviors, as well as their fire risk and hazards. Whether larger cells are more dangerous because of their greater total energy, or may actually have an inherent safety advantages due to their smaller specific surface area and large thermal inertia (Hong et al., 2025). Consequently, whether post-venting emergency immersion cooling can be used for larger, higher-energy-density battery cells remains unknown, highlighting a critical knowledge gap.

This study investigates post-venting immersion cooling of Li-ion batteries as an emergency measure to prevent thermal runaway in cylindrical cells of different scales (18650, 21700, 32650, etc.) and volumetric energy density ranging from 447 to 1190 Wh/L. Central to the analysis is a proposed theoretical framework that simulates the prevention of thermal runaway via the competition between internal heat generation and surface immersion cooling. This work first identifies three distinct failure modes that challenge the bias of "high energy equals high fire risk", highlighting the safety benefits of cells with greater thermal inertia. Second, the minimum volumes of immersion cooling are defined to prevent the onset of battery thermal runaway. Finally, a novel dimensionless criterion is derived for different battery cells, consolidating diverse datasets into a universal thermal safety map with physics-based design guidance.

2. Experimental method

2.1. Battery cell

To investigate the size-dependent battery thermal safety boundaries, a comprehensive experimental matrix was established that covers 5 standard cylindrical cell types: 18650, 21700, 26650, 26700, and 32650. These cells represent a wide range of energy densities (~447–1190 Wh/L) and power capabilities. Detailed specifications of the tested cells are summarized in Table 1. Prior to testing, all cells were charged to 100% State of Charge (SOC) using a constant-current constant-voltage (CC-CV) protocol at 0.5 C rate using a high-precision battery cycler (CT-4008 T-5 V/12 A, ± 6 mA, Neware), followed by a 24-hour rest period to ensure electrochemical equilibrium. The maximum cut-off voltage for charging is 4.20 ± 0.05 V, and the minimum cut-off voltage for discharging is 2.75 ± 0.05 V. The battery voltage will then be reviewed using the voltage curve.

2.2. Experimental apparatus

The experimental setup, designed to simulate external thermal propagation and evaluate immersion cooling suppression, is schematically illustrated in Fig. 2(a). The photos of tested 18650, 21700, 26650, 26700 and 32650 cylindrical cells with different energy capacities are shown in Fig. 2(b).

2.2.1. External heating system (inductive heating)

Unlike conventional oven heating or nail penetration, a high-frequency induction heating module (150 W, ~50–100 kHz) was employed. A helical copper coil with an inner diameter of 50 mm and a copper tube used as the coil with an outer diameter of 6 mm, and a total of 7 turns, was used to generate an alternating magnetic field (IEC, 2022; Zhang et al., 2025b). This setup induces eddy currents specifically within the steel casing of the battery (Skin Effect), creating a controllable, high-flux surface heat source that mimics the impingement of thermal runaway from adjacent cells. A direct current (DC) power supply is used to maintain constant heating power and pre-calibrate the current and voltage parameters.

2.2.2. Immersion coolant and cooling system

The cell was housed in a custom-designed transparent acrylic container. A non-conductive dielectric fluid (HFE-7200) served as the coolant (Zhang et al., 2025b). The properties of the coolant are summarized in Table 2. A precision nozzle was positioned to maintain the coolant level or facilitate injection.

2.2.3. Data acquisition

Temperature evolution was recorded by a data logger (HIOKI LR8431 - 30) at a sampling rate of 1 Hz. A video camera (SONY RX10III) was positioned to capture the macroscopic failure morphology (e.g., venting, ejection, or fire). All experiments were conducted inside a room with an ambient temperature of 28 ± 3 ℃, ambient pressure of 101 kPa, and good ventilation conditions. To improve the transient thermal response, K-type thermocouples with a diameter of 0.5 mm were used to measure the battery surface temperature (T_{surf}), ambient temperature (T_a) and magnetic field compensated temperatures (T_m, ±0.1 ℃).

2.3. Testing procedures

The experiments were divided into two main groups to decouple the effects of battery geometry and cooling.

- **Group 1: Standard Heating (Baseline).** Cells were subjected to continuous inductive heating without coolant until venting occurred. This group established the inherent failure modes (e.g., Meltdown vs. Safe venting) and reference critical temperatures (T_{tr} and T_{max}).
- **Group 2: Post-venting Immersion Cooling Limits.** Cells were submerged in the dielectric fluid with varying coolant-to-cell volume ratios (Φ), ranging from 0 (dry) to 1/2. The ratio Φ is defined as V_c/V_B. The induction heater was activated at a constant power output until the cell entered venting.

Table 1
Specifications of the commercial Li-ion cells tested in this study.

Cell Type	Cathode material	Capacity (Ah)	Normal Voltage (V)	Mass, m (g)	Volume, V (mL)	Specific surface area, SSA (m^2/L)	Vol. energy density, ε (Wh/L)	Mass energy density (Wh/kg)
32650	LFP	6.5	3.7	160.0	52.3	0.156	460	150
26700	LFP	5.0	3.7	97.0	37.2	0.182	498	191
26650	LFP	6.5	3.7	86.0	34.5	0.185	697	280
	NCM	6.0	3.7	90.0	34.5	0.185	643	247
	LFP	5.0	3.7	93.6	34.5	0.185	522	192
21700	NCM	7.8	3.7	69.0	24.3	0.219	1190	418
		5.8	3.7	73.7	24.3	0.219	885	291
		5.0	3.7	68.1	24.3	0.219	763	272
		4.0	3.7	65.5	24.3	0.219	610	226
18650	NCM	3.5	3.7	48.0	16.5	0.253	732	252
		3.0	3.7	45.9	16.5	0.253	659	238
		2.6	3.7	45.1	16.5	0.253	582	213
		2.0	3.7	42.5	16.5	0.253	447	174

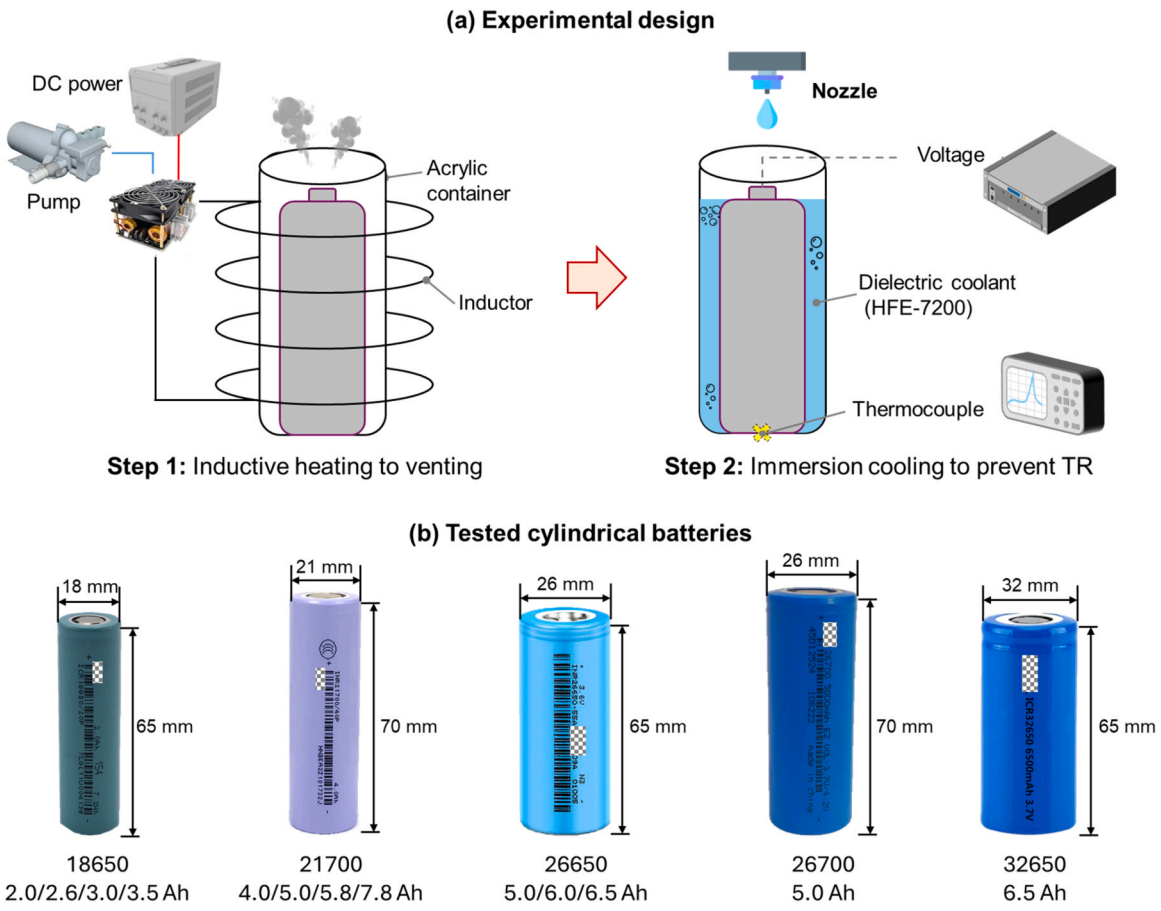

Fig. 2. (a) Diagram of the experimental design. Step 1: inductive heating of the battery to venting, and Step 2: the immersion cooling for preventing thermal runaway; and (b) photos of tested cylindrical batteries.

Table 2
Properties of immersion coolant: non-conductive dielectric fluid (HFE-7200).

Property	Value
Boiling point at 1 atm (°C)	76
Specific heat (J/kg/K)	1210
Coefficient of thermal expansion(1/°C)	0.0016
Thermal conductivity (W/m/K)	0.068
Latent heat of vaporization (kJ/kg)	125
Density (kg/m^3)	1430
Surface tension (N/m)	0.0136
Kinematic viscosity (mm^2/s)	0.41
Freezing point (°C)	-138

In this study, thermal runaway is defined as the instant when the temperature rise rate ($\frac{dT}{dt}$) exceeds 10 ℃/s (Feng et al., 2015), accompanied by visible smoke venting. After the battery safety valve is opened, immediately stop heating, remove the induction coil, and add dielectric coolant to the PMMA container by drip-filling in 2 s. The container is a bottomed and uncovered cylindrical container made of PMMA, the diameter of which is selected according to the volume ratio Φ (from 1/16 - 1/2). After heating, the experimental phenomena and cell temperature were observed continuously. The experiment was terminated once the temperature of all cells was sufficiently reduced to a safe value of approximately 50°C for processing. To minimize experimental uncertainty, each case was repeated at least twice.

3. Results

3.1. Post-venting modes and risks

To systematically decouple the effects of cell geometry and energy density on thermal safety, a comprehensive experimental matrix comprising 13 distinct commercial cell models was constructed. As detailed in Table 3, these samples span 5 standard cylindrical formats, covering a wide range of energy densities. Based on the experimentally observed failure behaviors, the tested cells are stratified into three distinct risk levels in Table 3. Under identical inductive external heating, battery cells exhibited three different failure modes: (I) High Risk of TR with Internal Meltdown, (II) Low Risk of TR with Lid Open, and (III) No Risk of TR with Safe Venting.

Fig. 3 illustrates some typical experimental phenomena of externally heated battery cells with different post-venting risks of thermal runaway, as compared in Table 3 (also see Video S1). The thermal behavior varied significantly depending on the cell format and application of immersion cooling. Fig. 3(a) displays the High-risk Model I (Internal Meltdown) using the 18650 cell (3.5 Ah) without cooling. Following the safety valve opening at 1′48", the cell entered a self-heating phase that rapidly self-heats to thermal runaway. This mode has intense flames and high temperatures, causing the cell case to turn red. Larger-volume cells exhibited different failure mechanisms.

Fig. 3(b) shows the 21700 cell (5.8 Ah) demonstrated a Low-risk Model II (Lid Open with partial jelly roll ejection). The rapid accumulation of internal pressure caused the cell cap to burst, resulting in the ejection of jelly roll. The ejection also takes a huge amount of heat away, which leads to a lower surface temperature. Fig. 3(c) shows the largest cell, 32650 (6.5 Ah), tested in this study, which exhibited the No-risk

Table 3
Characteristics of the tested Li-ion batteries (SOC = 100%) and their intrinsic safety classification, where the mass losses for Thermal Runaway (TR) and No Thermal Runaway (NTR) are compared.

Cell Type	Capacity (Ah)	TR risk ψ (%)	Mass Loss (%)	TR model and risk rank	Post Exp.
32650	6.5	0	4.3	III: No risk (Safe Venting)	
26700	5.0	0	7.1	III: No risk (Safe Venting)	
26650	6.5	40	5.6 (NTR)/ 80.6 (TR)	II: Low risk (Lid Open)	
	6.0	60	5.2 (NTR)/ 39.7 (TR)	I: High risk (Internal Meltdown)	
	5.0	40	5.6 (NTR)/ 39.3 (TR)	I: High risk (Internal Meltdown)	
21700	7.8	40	10.4 (NTR)/ 86.4 (TR)	II: Low risk (Lid Open)	
	5.8	20	7.1 (NTR)/ 83.9 (TR)	II: Low risk (Lid Open)	
	5.0	20	11.6 (NTR)/ 84.4 (TR)	II: Low risk (Lid Open with jelly-roll ejection)	
	4.0	100	59.8	I: High risk (Internal Meltdown)	
18650	3.5	100	39.3	I: High risk (Internal Meltdown)	
	3.0	100	55.4	I: High risk (Internal Meltdown)	
	2.6	0	6.7	III: No risk (Safe Venting)	
	2.0	0	6.6	III: No risk (Safe Venting)	

Note: The two values for the mass loss represent specific typical test cases.

Model III (Safe Venting), where the temperature naturally decayed after the safety valve opened. This mode exhibited a mitigation through venting of thermal runaway. Fig. 3(d) demonstrated the effectiveness of immersion cooling on an 18650 cell (see Video S2). By injecting a small amount of dielectric coolant (1/2 vol of battery cell) immediately after the safety valve opened, the onset of the thermal runway was stopped (prevention of the violent thermal runaway transition and visible flaming fire) and the cell integrity looked similar to the No-risk Model III.

Supplementary material related to this article can be found online at doi:10.1016/j.psep.2026.108730.

Fig. 4(a) shows the thermal behaviors of typical cells under standard heating. While the high-power cell (18650 3.5 Ah) exhibits irreversible thermal runaway after venting, the larger-volume cell (32650 6.5 Ah) enters a self-limiting "safe venting" state. Surprisingly, the highest-energy-density cell (21700 5.8 Ah) does not explode most violently; instead, it shows a delayed response, challenging the conventional bias of "higher energy = higher risk" under external heating conditions.

As illustrated in Figs. 3(a-c) and 4(a), the thermal responses can be categorized into three distinct models based on the competition between internal pressure buildup and casing structural integrity

Model I (High Risk of TR with Internal Meltdown): Observed primarily in high-power, small-format cells (e.g., 18650 3.5 Ah). These cells exhibit an extremely rapid temperature rise rate ($\frac{dT}{dt} > 100\ ℃/s$) with a sharp peak exceeding 600 °C. The failure is characterized by a complete internal collapse before the casing can effectively vent, leading to the most severe thermal outcome.

Model II (Low Risk of TR with Lid Open): Observed in medium-risk cells (e.g., 21700 5.8 Ah). The failure involves a violent ejection of the jellyroll. Notably, the ejection process physically removes a significant portion of the reacting mass, resulting in a sharp drop in the measured casing temperature.

Model III (No Risk of TR with Safe Venting): Surprisingly, larger or higher-capacity cells (e.g., 32650 6.5 Ah) exhibited the mildest failure mode. Despite their high total energy, these cells showed a "self-terminating" temperature profile. The thick steel casing and large diameter created a substantial thermal gradient, causing the safety valve to open and release internal pressure before the core reached the critical thermal runaway temperature.

To further quantify the stability margin of the larger cell, a separate test with continuous post-venting heating was conducted under the occurrence of thermal runaway. Taking a 32650 6.5 Ah battery as an example. It required around an additional 120 s of extra heating post-venting to finally trigger the onset of thermal runaway. This huge energy barrier confirms that the 32650 6.5 Ah cell possesses a significantly wider safety window compared to the smaller cell (18650 3.5 Ah), which led to thermal runaway upon venting without extra energy input.

Fig. 4(b) confirms the universal feasibility of immersion cooling for battery cells of different scales and energy densities. When subjected to the same trigger but submerged in dielectric fluid (with a sufficient volume ratio, e.g., $\Phi = 1/2$), the disparate failure modes observed in Fig. 4(a) are unified into a single safe state. Regardless of whether the cell was prone to meltdown (Mode I: High risk) or safe venting (Mode III: No risk), the surface temperature was effectively maintainednear the dielectric coolant's boiling point (~ 76 ℃ for HFE-7200). This result demonstrates that phase-change cooling acts as a reliable safety barrier. It effectively mitigates the intrinsic risks of high-energy chemistry, validating the fundamental feasibility of immersion cooling as a global solution for diverse cell formats.

Fig. 5 shows a multi-dimensional risk diagram as a function of (a) cell specific surface area (SSA) and (b) cell mass loss. Fig. 5(a) maps the SSA against the volumetric energy density, providing a global view of the safety landscape. The data points are categorized by risk level (solid marker: High Risk; half-solid marker: Low Risk; marker with cross: No Risk), and the background colors delineate three distinct zones. The geometric safety threshold indicates a trade-off mechanism. Within the no-risk zone, a larger specific surface area enables the battery to tolerate higher energy densities, owing to improved thermal management efficiency. As energy density increases, the battery enters the melt zone, characterized by a high peak temperature.

When the battery size becomes larger (lower SSA), thermal runaway becomes a probabilistic event, and even if thermal runaway occurs, its peak temperature is slightly lower than that of batteries in the high-risk zone. This is because larger-sized batteries have greater thermal inertia, and when external heating triggers thermal runaway, there is a larger temperature difference between the core and the battery surface, which protects the battery from thermal runaway. Interestingly, at ultra-high energy densities (> 700 Wh/L), the failure mode shifts to Low-risk Model II (Lid open with partial jelly-roll ejected from cell). The ejection of jelly roll acts as a passive cooling mechanism, removing the enthalpy of the reactants and unexpectedly reducing the temperature of

Fig. 3. Snapshots of different battery failure modes (SOC 100%), (a) 18650 3.5 Ah, Model I (meltdown) with thermal runaway, (b) 21700 5.8 Ah, Model II (lid open) with injection of jelly roll, (c) 32650 6.5 Ah, Model III (safe venting) without thermal runaway, and (d) the immersion of dielectric liquid (1/2 vol of battery cell) to stop TR onset of 18650 3.5 Ah (see Videos S1-S2).

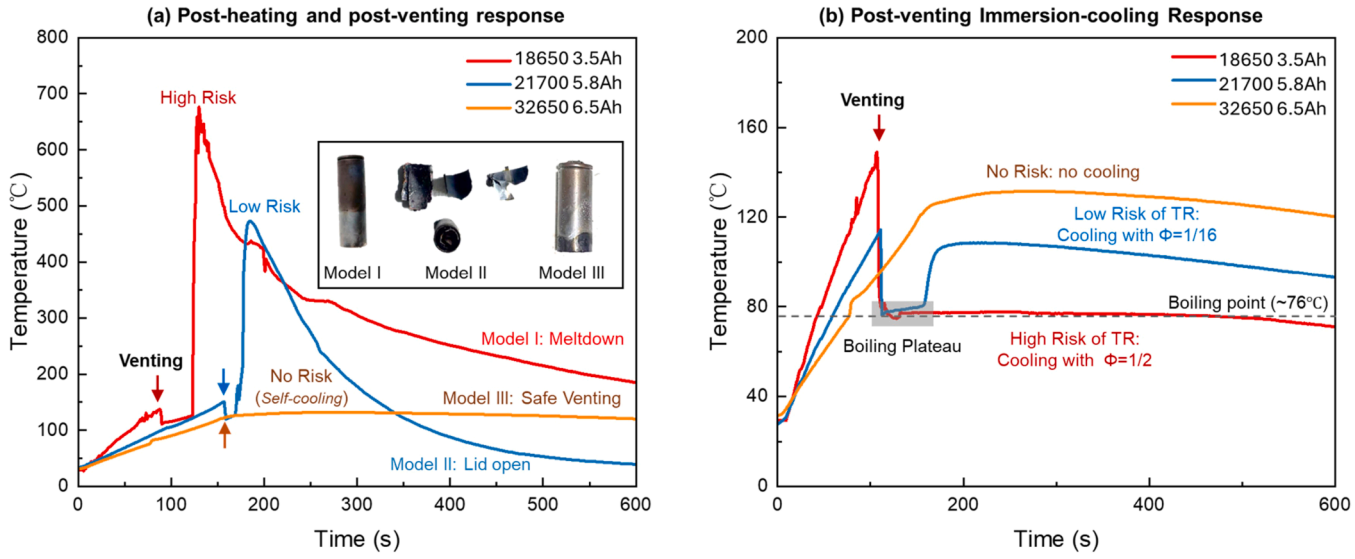

Fig. 4. Temperature curves of different battery venting behaviors (SOC = 100%) (a) post-heating and post-venting response with three failure modes and (b) post-venting Immersion-cooling Response.

the casing.

Fig. 5(b) illustrates the thermodynamic mechanism behind this phenomenon by plotting mass loss against energy density. The color gradient reveals that safety for high-energy cells is governed by a critical "enthalpy removal threshold" at approximately 70% mass loss. For cells with moderate mass loss (20–70%), the ejection is incomplete. While sufficient to destroy internal integrity, it fails to dissipate reaction heat. Consequently, these cells (dark red/black points) remain thermally "trapped," leading to severe meltdown with peak temperatures exceeding 500 °C. Only when the energy density drives the mass loss beyond 70% does the "sacrificial cooling" effect dominate. The violent ejection of over two-thirds of the cell mass acts as a massive heat dissipation, effectively carrying away the reaction enthalpy. This explains the paradoxical observation in Fig. 5(a): high-energy cells can "escape" the high-risk zone and land in the low-risk zone, provided they eject enough mass to cross this safety threshold.

These three naturally clustered areas confirm the "enthalpy removal" hypothesis. From a thermodynamic perspective, the total heat accumulated in the casing (Q_{case}) is the difference between heat generation (Q_{gen}) and heat removal as:

$$Q_{case} = Q_{gen} - (Q_{diss} + Q_{eject}) \quad (1)$$

For High-risk Model I (Meltdown), the ejection term Q_{eject} is small, trapping the reaction heat inside the casing. In contrast, for Lower-risk Model II/III, the violent ejection of the jellyroll and electrolyte physically transports a massive amount of high-temperature matter out of the system. This sacrificial mass loss effectively acts as a rapid "heat dissipation", preventing the remaining casing from reaching the threshold temperature required to ignite adjacent cells. Thus, for high-energy density cells, material ejection is not merely a failure consequence, but an passive cooling mechanism that limits thermal runaway propagation risk.

3.2. *Dynamic suppression via immersion cooling*

For the external heating of a larger-volume battery cell, it takes a

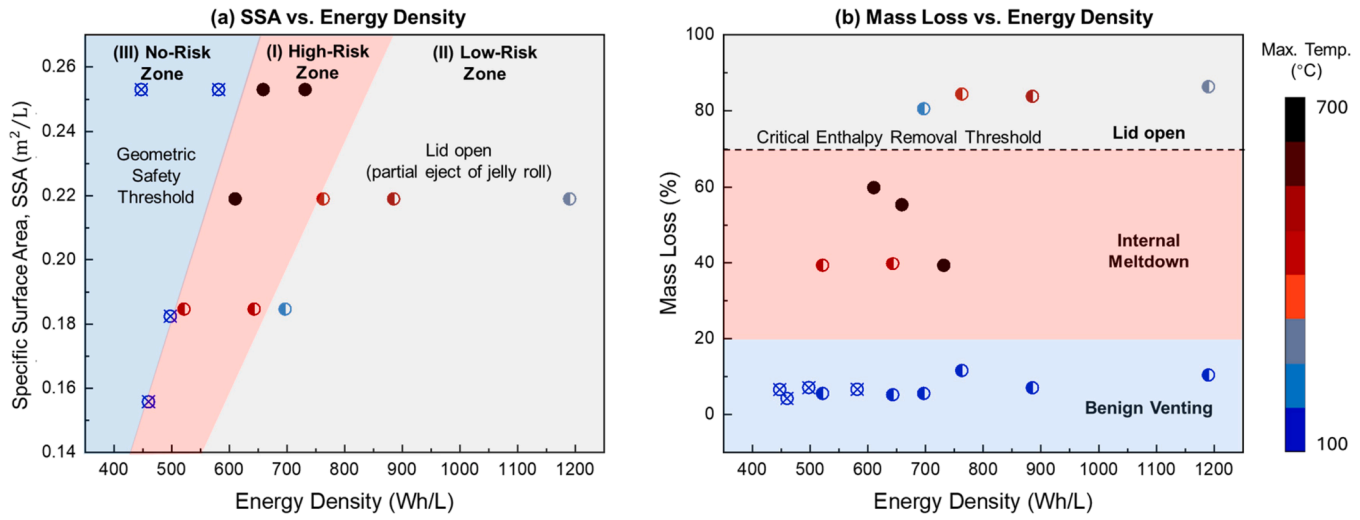

Fig. 5. Cylindrical battery thermal-runaway risks and modes: (a) the thermal safety phase diagram and (b) The sacrificial cooling mechanism.

longer time to reaching the venting point. This study investigates how the emergency immersion cooling leverages the time window after venting to prevent the onset of thermal runaway. Fig. 6 details the transient temperature responses under immersion cooling for cylindrical cells with different thermal-runaway risks. A characteristic "boiling plateau" is observed near the coolant's boiling temperature (T_{boil} = 76 ℃), signifying the dominance of nucleate boiling heat transfer ($h \sim 10^4$ W/m^2/K (Zhang et al., 2025b)). However, the plateau's evolution over time reveals the finite nature of the cooling capacity. Initially, the surface temperature is rigidly clamped at T_{boil}, effectively suppressing the rapid casing temperature rise seen in dry tests. As the coolant is consumed via evaporation, the liquid transits the heat transfer mode from boiling back to gas convection. Consequently, the temperature exhibits a secondary rise. For large batteries (low-risk mode, 26700 5.0 Ah as an example), only a very small amount of coolant ($\Phi < 1/16$) is usually needed to completely eliminate the risk of thermal runaway.

The thermal response of the high-power cell (18650 3.5 Ah) reveals a critical sensitivity to the coolant volume, highlighting the competition between internal self-heating and immersion cooling. As shown in Fig. 6 (b), the temperature profiles exhibit distinct behaviors depending on the volume ratio (Φ). With minimal coolant, the boiling plateau is transient. The limited liquid inventory is rapidly consumed before the cell's internal reaction heat is exhausted. Consequently, the temperature breaks away from the boiling plateau and rises up exponentially, indicating that the cooling capacity was overwhelmed by the high self-heating rate, failing to prevent thermal runaway. With adequate coolant, the boiling plateau is sustained for a sufficient duration. This abrupt transition underscores that for high-energy density cells, the cooling system design must account for a quantitative critical cooling limit, rather than relying on generic immersion.

Fig. 7 summarizes a peak cell temperature under standard (red bars) and immersion (blue bars) conditions, where the cases of continuous post-venting heating (grey hatched bars) are included as well. The cooling intervention manifests in three distinct degrees of effectiveness:

(1) Mitigation (High-risk, internal meltdown). For the most aggressive cells, the thermal runaway outcomes are similar, regardless of under standard heating or continuous post-venting heating. Under standard heating, these cells deterministically enter thermal runaway. Immersion cooling may not fully prevent internal

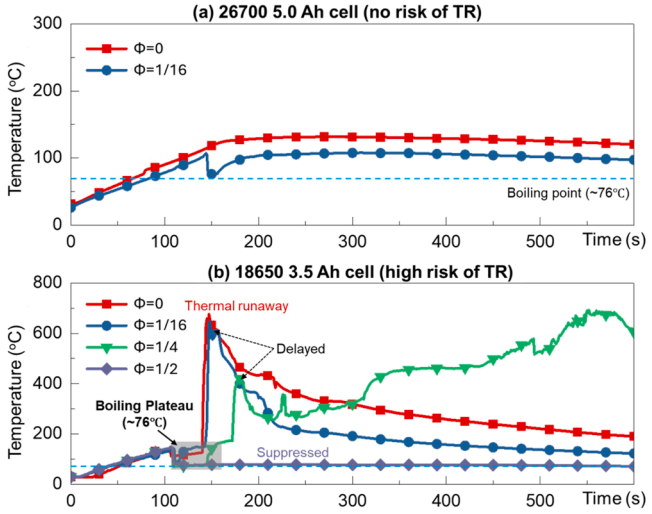

Fig. 6. Battery post-venting dynamics under different coolant volumes: (a) 26700 5.0 Ah cells without risk of thermal runaway and (b) 18650 3.5 Ah cells with high-risk of thermal runaway, where all cells are fully charged.

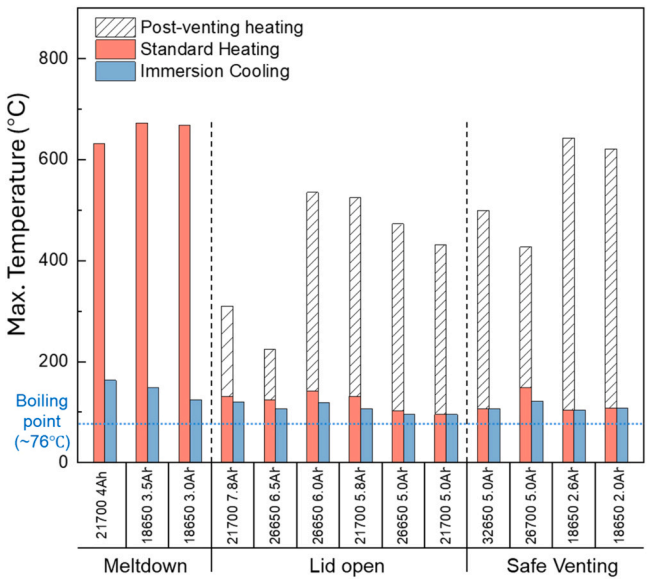

Fig. 7. Statistical summary of battery thermal safety margins for standard heating, post-venting heating, and post-venting immersion cooling, where the boiling point of dielectric HFE-7200 is 76 ℃.

material degradation. But with sufficient coolant, the cooling system acts as a "mitigation" strategy to bring the temperature down to the boiling plateau.

(2) Suppression (Low-risk, lid open). For medium-risk cells, the transition to thermal runaway is strictly probabilistic. The grey hatched bar represents the scenario where thermal runaway does occur (high risk outcome). The red bar represents the scenario observed in our standard baseline tests where the cell successfully ejected material or vented without initiating full thermal runaway (low risk outcome). Since the failure is random under dry conditions, immersion cooling provides a critical "suppression" function, shifting the probability of failure from random to zero.

(3) Redundancy (No-risk, safe venting). For these inherently safer cells, the red bar is inherently low (~120 °C), confirming that standard heating cannot trigger thermal runaway. The grey hatched bar here represents a distinctly different condition: continuous heating. It indicates that thermal runaway is only possible when the cell is subjected to sustained energy input far beyond the venting point. In this case, immersion cooling serves as a "redundancy," ensuring safety even under extreme abuse conditions where intrinsic geometric safety might be overwhelmed.

3.3. Critical cooling limits and safety map

While Section 3.2 verified the feasibility of suppression, the sensitivity observed in high-power cells (Fig. 6) raises a critical engineering question: What is the minimum coolant volume required to guarantee safety? To answer this, this study performed a quantitative sensitivity analysis on the high-risk cells, varying the Φ from 0 to 1/2.

Fig. 8(a) maps the maximum cell temperature against the dielectric coolant-cell volume ratio (Φ). A distinct "safety cliff" is evident for all cells: below a specific threshold (Φ_{min}, the lower safety limit), the cooling capacity is insufficient, resulting in thermal runaway with a cell temperature above 400 °C. Above this threshold, the temperature is successfully clamped. Crucially, this critical threshold is not universal but cell-dependent and coolant-dependent (Zhang et al., 2025b). The 18650 3.0 Ah cell is suppressed at $\Phi_{min} = 1/8$ (conservative estimation). The larger 21700 4.0 Ah cell requires a higher ratio of $\Phi_{min} = 1/4$. The high-energy-density 18650 3.5 Ah cell demands the highest ratio of $\Phi_{min} = 1/2$ to prevent thermal runaway. This thermal-runaway risk ranking (18650 3.5 Ah > 21700 4.0 Ah > 18650 3.0 Ah) strongly suggests that the minimum coolant volume scales with the total stored energy or energy density rather than just cell size (or volume). Despite employing the same structure as the 3.0 Ah battery, this high-energy-density 3.5 Ah battery requires a larger proportion of enthalpy absorption method to neutralize the heat it releases due to its more densely packed reactive materials.

Fig. 8(b) elucidates the physical mechanism behind these thresholds. The Y-axis represents the time window (time from venting to thermal runaway, Δt_w). A clear positive correlation exists: increasing coolant volume extends the duration of the "boiling clamp". The annotation "bigger energy capacity → longer self-heating stage" highlights the root cause: high-energy cells (e.g., 21700 4.0 Ah and 18650 3.5 Ah) sustain a prolonged heat release. Consequently, suppression is fundamentally an endurance race: the coolant's latent heat capacity must last longer than the cell's active heat generation phase. For instance, at $\Phi = 1/8$, the 18650 3.0 Ah cell is safe because the boiling duration covers its reaction window. However, for the 21700 4.0 Ah cell at the same ratio, the coolant is consumed quickly, leading to thermal runaway.

To translate the experimental findings into a practical engineering guideline, we synthesized the critical cooling limits of all tested cells into a unified safety map, as shown in Fig. 9. By mapping the critical dielectric coolant ratio against the specific surface area, a distinct geometric scaling law emerges. Contrary to the expectation that high-SSA cells dissipate heat more efficiently, the results reveal that they actually demand a significantly higher coolant consumption to suppress thermal runaway. Small-format cells (right side, e.g., 18650 s) exhibit

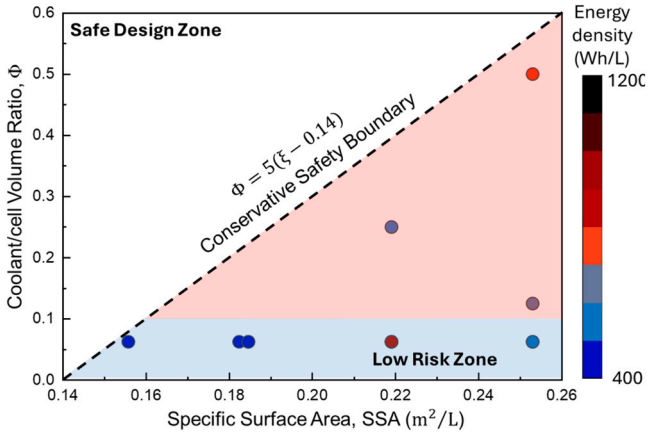

Fig. 9. Multi-dimensional battery safety map correlating critical cooling (immersion by dielectric HFE-7200) requirements with cell geometry and energetics.

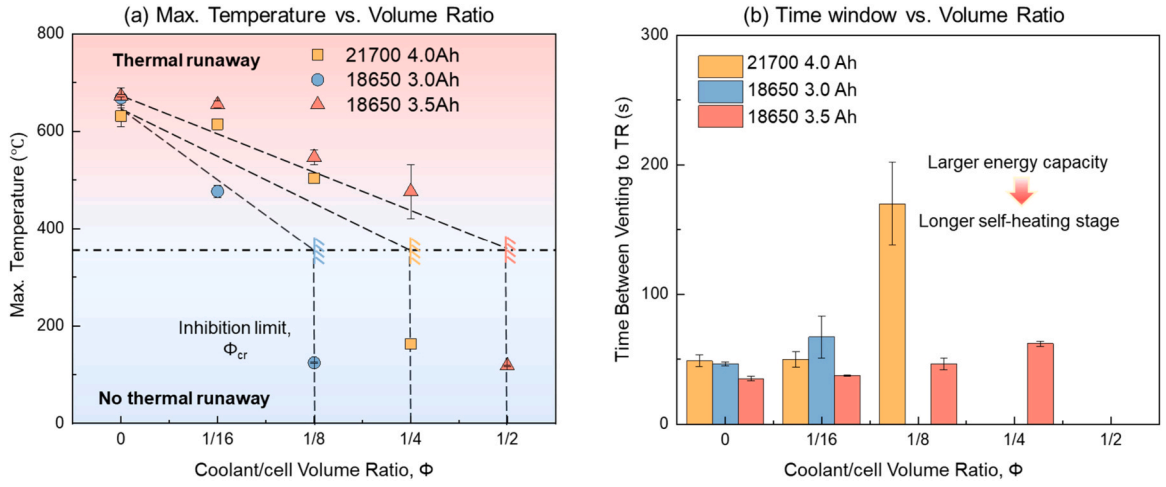

Fig. 8. Determination of critical cooling limits with dielectric HFE-7200: (a) Max. temperature vs. volume ratio and (b) time window vs. volume ratio, where all battery cells are fully charged.

rapid reaction rate due to their low thermal mass. This internal self-heating exceeds the surface cooling rate, necessitating a high coolant volume ratio to successfully quench the reaction. Larger cells (e.g., 32650) benefit from its larger thermal inertia. The cell's thermal inertia suppresses the reaction rate, allowing for successful suppression with minimal coolant.

To provide a deterministic criterion for thermal management design, we defined a "Conservative Safety Boundary" (dashed line in Fig. 9). This boundary represents the upper envelope of the experimental data, delineating the necessary coolant volume to guarantee safety under worst-case inductive heating scenarios. For any given cell geometry, a thermal management system must be dimensioned such that the coolant volume ratio falls within the "Safe Design Zone" (above the dashed line). This map effectively decouples the complex internal chemistry from the system design. Engineers can determine the minimum safety redundancy solely based on the cell's geometric parameter, avoiding the need for costly trial-and-error testing for every new cell model. The empirical formula used for the engineering design of post-venting emergency cooling can be referenced as follows:

$$\Phi_{\min} = 5(SSA - 0.14) \tag{2}$$

Fig. 9 establishes a robust, geometry-based standard. It confirms that while high-energy chemistry dictates the potential hazard, the cell scale and shape (reflected by SSA) will affect the ease of post-venting cooling and suppression. The proposed safety boundary provides a simple yet effective tool for sizing immersion cooling systems for next-generation battery packs. However, different battery orientations can affect heat and mass transfer processes. For example, horizontal orientation might lead to vapor trapping on the lower surface of the cell, potentially reducing the heat transfer coefficient. To ensure redundancy in engineering applications, we recommend applying a safety factor of 1.2–1.5 to $\Phi_{\min}$ in practical use.

4. Discussion

To unify the disparate behaviors observed in Fig. 9, this study formulated a physical model describing the thermal competition within the cell, as illustrated in Fig. 10. The fate of a battery after venting is determined by the competition between internal heat generation (or self-heating $\dot{Q}_{gen}$) and heat dissipation ($\dot{Q}_{diss}$). Driven by the exothermic decomposition of the battery materials. Its magnitude depends on the mass (m) and the self-heating reaction rate. Heat dissipation is provided by the boiling of the dielectric fluid. Its magnitude depends on the surface area (A) and the heat transfer coefficient (h). Under dry conditions (Fig. 10a), air cooling is insufficient to balance $\dot{Q}_{gen}$, leading to thermal runaway. Immersion cooling (Fig. 10b) introduces a high-efficiency removal channel via nucleate boiling. Early mitigation is achieved only when the boiling heat flux can extract the internal enthalpy faster than it is generated, ensuring that the cell temperature is below the onset point of thermal runaway ($T_{TR,0}$).

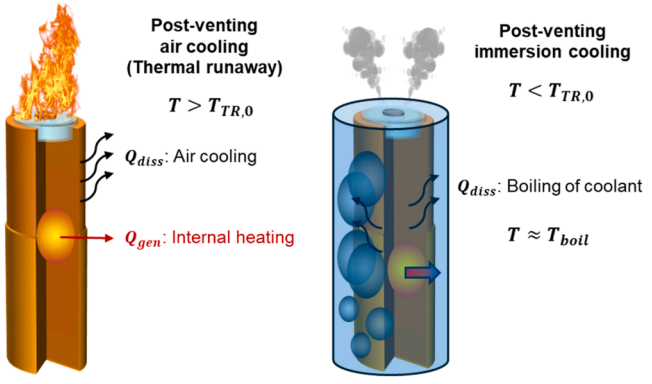

Fig. 10. Model for the competition of battery post-venting self-heating and immersion cooling.

Based on the physical model, we derive the critical cooling criterion mathematically. Considering the time window (Δt_w) from venting to the onset of thermal runaway (as defined in Fig. 8b), the average internal heat generation rate ($\dot{Q}_{gen}$) required to heat the battery mass (m_B) from the venting temperature (T_{vent}) to the thermal runaway trigger temperature ($T_{TR,0}$) can be approximated as:

$$\dot{Q}_{gen} \bullet \Delta t_w \approx m_B c_{p,B} \left(T_{TR,0} - T_{vent}\right) \tag{3}$$

Rearranging this, the heat generation power scales inversely with the time window:

$$\dot{Q}_{gen} = \frac{m_B c_{p,B}}{\Delta t_w} \left(T_{TR,0} - T_{vent}\right) \propto \frac{1}{\Delta t_w} \tag{4}$$

where $c_{p,B}$ is the specific heat capacity of the battery. This equation mathematically confirms that cells with faster self-heating kinetics (shorter Δt_w) exhibit higher instantaneous heat generation power.

To prevent thermal runaway, the surface cooling power must balance this generation power ($\dot{Q}_{diss} = \dot{Q}_{gen}$). The boiling heat transfer rate is given by:

$$\dot{Q}_{diss} = A_B h_c \left(T_{surf} - T_{boil}\right) \tag{5}$$

where A_B is the surface area, h_c is the boiling heat transfer coefficient, T_{surf} is the battery surface temperature and T_{boil} is the coolant boiling point.

The total energy that must be absorbed by the coolant is limited by the coolant's latent heat of vaporization (ΔH_{ev}). The minimum volume of coolant ($V_{c,min}$) required to absorb the generated heat over the duration Δt_w is:

$$\rho_c V_{c,min} \Delta H_{ev} = \dot{Q}_{gen} \bullet \Delta t_w = \dot{Q}_{diss} \bullet \Delta t_w \tag{6}$$

Substituting $\dot{Q}_{diss}$, we have

$$\rho_c V_{c,min} \Delta H_{ev} = \left[A_B h_c \left(T_{surf} - T_{boil}\right)\right] \bullet \Delta t_w \tag{7}$$

Dividing both sides by the battery volume (V_B) to introduce the dimensionless ratio of coolant-cell volume ratio ($\Phi_{\min}$) as

$$\Phi_{\min} = \frac{V_{c,min}}{V_B} = \frac{A_B}{V_B} \bullet \Delta t_w \bullet \frac{h_c \left(T_{surf} - T_{boil}\right)}{\rho_c \Delta H_{ev}} \propto SSA \bullet \Delta t_w \tag{8}$$

where the material properties (ρ_c, ΔH_{ev}, h_c) are constants, and the specific surface area is

$$SSA = \frac{A_B}{V_B} \tag{9}$$

It is assumed that the time window (Δt_w) between venting and thermal runaway is related to the battery energy density (ε). Then, the scaling law simplifies to

$$\Phi_{\min} \propto SSA \bullet \varepsilon \tag{10}$$

This derived scaling law reveals that the difficulty of emergency cooling is fundamentally dictated by the coupling of geometric efficiency (i.e., SSA) and energetic potential (ε). A higher SSA promotes the coolant evaporation, increasing the instantaneous evaporation rate required to clamp the surface temperature. A higher ε implies a larger reservoir of reaction enthalpy, extending the duration of the thermal event and requiring a larger total coolant inventory to prevent the boil out. It accounts for the worst-case coupling of a high consumption rate (high SSA) and long burn duration (high ε), providing engineers with a deterministic tool to size immersion cooling systems using only standard datasheet parameters, without the need for destructive testing to determine reaction kinetics.

For high energy density modules, the coolant consumption must be

sized not just for one cell, but for the total energy of a "trigger group," effectively requiring a safety margin to prevent the failure of neighboring cells. Moreover, the practical application to square formats introduces new challenges, such as significant internal thermal gradients due to their increased thickness and different mechanical responses of the aluminum casing under internal pressure compared to cylindrical steel shells. These factors suggest that while the fundamental physics holds, engineering designs for square batteries may require additional shape correction factors or higher safety redundancies to account for internal-to-external heat transfer delays. This will be a key focus for the next phase of work.

5. Conclusions

This study quantifies the limits (minimum coolant usage) of post-venting immersion cooling with a dielectric liquid (HFE-7200) for cylindrical Li-ion batteries with sizes ranging from 18650 to 32650 and energy densities from 447 to 1190 Wh/L. The key findings are summarized as follows:

(1) Failure modes: We identified three geometry-dependent failure models: (I) High risk with internal meltdown, where high-power small cells (heating rate ~1.0 °C/s) inevitably spiral to peak temperatures > 600 °C; (II) Low risk with Lid open, where the violent expulsion of jelly-roll material provides passive enthalpy removal to mitigate risks; and (III) No risk with safe venting, where larger-volume cells benefit from thermal inertia (heating rate ~0.4 °C/s) to self-terminate without thermal runaway.
(2) Cooling mechanism: Immersion cooling effectively clamps the casing temperature at the boiling point (~76 °C). However, a "safe regime" exists: preventing the onset of thermal runaway for high-risk cells requires a minimum coolant-to-cell volume ratio of $1/4 < \Phi_{\min} < 1/2$, whereas for low-risk cells (lid open/safe venting), it only required $\Phi_{\min} < 1/16$.
(3) Critical threshold: We derived a physics-based scaling law $\Phi \propto SSA \bullet \varepsilon$, which reveals that suppression difficulty is dictated by a coupling mechanism. A conservative safety boundary, $\Phi_{\min} \approx 5(SSA - 0.14)$ was obtained. These formulas allow engineers to determine the minimum coolant inventory solely from cell geometry and energy density, without costly and destructive testing.

In summary, this work bridges the gap between intrinsic cell attributes and extrinsic suppression limits. It demonstrates that thermal safety is deterministically achievable when the coolant inventory is dimensioned to outlast the coupled kinetic and energetic discharge of the battery.

CRediT authorship contribution statement

Yuying Chen: Formal analysis, Data curation. **Yichao Zhang:** Resources, Data curation. **Feiyu Guan:** Formal analysis, Data curation. **Lei Zhang:** Writing – original draft. **Shi Liu:** Resources, Project administration. **Congliang Ye:** Investigation, Data curation. **Yanhui Liu:** Formal analysis, Data curation. **Xinyan Huang:** Writing – review & editing, Supervision, Methodology, Conceptualization.

Declaration of Competing Interest

The authors declare that they have no known competing financial interests or personal relationships that could have appeared to influence the work reported in this paper.

Acknowledgements

This work is funded by grants from the Key R&D Program of Guangdong Province (2023B0909060004). XH also thanks PolyU Research Institute for Smart Energy (RISE) for its support.

Data availability

Data will be made available on request.

References

Ahmad, S., Liu, Y., Khan, S.A., Hao, M., Huang, X., 2023. Hybrid battery thermal management by coupling fin intensified phase change material with air cooling. J. Energy Storage 64, 107167. https://doi.org/10.1016/j.est.2023.107167.
Ahmad, S., Liu, Y., Khan, S.A., Shah, S.W.A., Huang, X., 2024. Modeling liquid immersion-cooling battery thermal management system and optimization via machine learning. Int. Commun. Heat. Mass Transf. 158, 107835. https://doi.org/10.1016/j.icheatmasstransfer.2024.107835.
Birbarah, P., Gebrael, T., Foulkes, T., Stillwell, A., Moore, A., Pilawa-Podgurski, R., Miljkovic, N., 2020. Water immersion cooling of high power density electronics. Int. J. Heat. Mass Transf. 147, 118918. https://doi.org/10.1016/j.ijheatmasstransfer.2019.118918.
Chen, L., Pereira, C., Pannala, S., Munjurulimana, D., Goossens, H., 2025. Mitigation of cylindrical lithium ion battery thermal runaway propagation with a flame retardant polypropylene thermal barrier. J. Energy Storage 108, 115042. https://doi.org/10.1016/j.est.2024.115042.
Chen, Y., Zhang, L., Zhang, Y., Zhou, Y., Zhang, Z., Lin, S., Wei, W., Huang, X., 2025. Underground fires induced by disposed Li-ion battery in peatland and landfill. Process Saf. Environ. Prot. 199, 107235. https://doi.org/10.1016/j.psep.2025.107235.
Cheng, Z., Min, Y., Qin, P., Zhang, Y., Li, J., Mei, W., Wang, Q., 2025. A distributed thermal-pressure coupling model of large-format lithium iron phosphate battery thermal runaway. Appl. Energy 378, 124875. https://doi.org/10.1016/j.apenergy.2024.124875.
Fan, H., Zhang, J., Zhang, G., Jiang, L., Jiang, W., He, Z., Wang, X., Wen, Y., Xu, N., 2026. Thermal runaway studies of power lithium-ion batteries under various abusive conditions: A review. Appl. Therm. Eng. 283, 128945. https://doi.org/10.1016/j.applthermaleng.2025.128945.
Fang, H., Gong, J., Li, L., 2025. Multi-objective optimization of cold plates for suppressing thermal runaway propagation within a lithium-ion battery module. Process Saf. Environ. Prot. 198, 107129. https://doi.org/10.1016/j.psep.2025.107129.
Feng, X., Sun, J., Ouyang, M., Wang, F., He, X., Lu, L., Peng, H., 2015. Characterization of penetration induced thermal runaway propagation process within a large format lithium ion battery module. J. Power Sources. https://doi.org/10.1016/j.jpowsour.2014.11.017.
Feng, X., Ouyang, M., Liu, X., Lu, L., Xia, Y., He, X., 2018. Thermal runaway mechanism of lithium ion battery for electric vehicles: A review. Energy Storage Mater. 10, 246–267. https://doi.org/10.1016/j.ensm.2017.05.013.
He, T., Gadkari, S., Zhang, T., Wang, Z., Liu, J., Mao, N., Bai, J., Cai, Q., 2024. Investigation of the internal physical and chemical changes of a cylindrical lithium-ion battery during thermal runaway. J. Clean. Prod. 434, 140548. https://doi.org/10.1016/j.jclepro.2023.140548.
Hong, Y., Wong, S.K., Jin, C., Zhang, M., Xu, C., Wang, H., Zheng, Y., Feng, X., Ouyang, M., 2025. Thickness-dependent of thermal runaway propagation velocity in lithium-ion batteries. Appl. Therm. Eng. 279, 127734. https://doi.org/10.1016/j.applthermaleng.2025.127734.
Hu, Q., Yang, H., Wu, H., Wang, X., Qian, X., Qi, S., Yuan, M., 2025. Numerical study on batteries thermal runaway explosion-venting risk and structural dynamic response in energy storage system container. Process Saf. Environ. Prot. 200, 107376. https://doi.org/10.1016/j.psep.2025.107376.
Huang, Z., Duan, Q., Li, J., Yang, F., Sun, J., Wang, Q., 2025. Experimental and numerical investigation of heating power effect on thermal runaway propagation within large-format lithium iron phosphate battery. J. Energy Storage 109, 115098. https://doi.org/10.1016/j.est.2024.115098.
IEC, 2022. Secondary cells and batteries containing alkaline or other non-acid electrolytes – Safety requirements for secondary lithium cells and batteries, for use in industrial applications. Int. Electrotech. Comm.
Liang, C., Lai, X., Shen, K., Zheng, Y., Xu, C., Ben-marzouk, M., Feng, X., Ouyang, M., 2026. Experimental study on immersion cooling for delaying thermal runaway propagation in lithium - ion battery modules. Process Saf. Environ. Prot. 206, 108333. https://doi.org/10.1016/j.psep.2025.108333.
Liu, Chunyuan, Zhang, G., Li, X., Yuan, D., Zhu, G., Liu, Changhui, 2025. Study on explosion venting efficacy of thermal runaway gases from lithium-ion batteries in a confined space: Impact of venting area. Process Saf. Environ. Prot. 203, 107876. https://doi.org/10.1016/j.psep.2025.107876.
Liu, J., Zhang, H., Chun, E., Jin, X., Zhao, K., Wang, Z., 2026b. Combustion behavior and quantitative analysis of fire risk for lithium-ion batteries with different SOC ☆. Appl. Therm. Eng. 288, 129613. https://doi.org/10.1016/j.applthermaleng.2025.129613.
Liu, J., Jin, X., Zhang, H., Zhao, K., Wang, Z., 2026a. Therm. Runaway Combust. LiFeO 4 LithiumIon.. Battery Induc. Electr. Therm. coupling Abus. 141.
Liu, T., Tao, C., Wang, X., 2020. Cooling control effect of water mist on thermal runaway propagation in lithium ion battery modules. Appl. Energy 267, 115087. https://doi.org/10.1016/j.apenergy.2020.115087.

Liu, Y., Aldan, G., Huang, X., Hao, M., 2023. Single-phase static immersion cooling for cylindrical lithium-ion battery module. Appl. Therm. Eng. 233, 121184. https://doi.org/10.1016/j.applthermaleng.2023.121184.

Liu, Y., Zhang, L., Ding, Y., Huang, X., Huang, X., 2024. Effect of thermal impact on the onset and propagation of thermal runaway over cylindrical Li-ion batteries. Renewable Energy 222, 119910.

Liu, Z., Zhu, Y., Li, R., Tao, C., Chen, Z., Liu, T., Li, Y., 2024. The experimental investigation of thermal runaway characteristics of lithium battery under different concentrations of heptafluoropropane and air. J. Energy Storage 84, 110828. https://doi.org/10.1016/j.est.2024.110828.

Mao, B., Lu, J., Zhang, Y., Chen, N., Lai, Z., Zhu, L., Cheng, R., Wen, J.X., 2025. International Journal of Heat and Mass Transfer Mitigating the cascading effects of thermal runaway and fire propagation in enclosed clusters of 18, 650-type lithium-ion batteries. Int. J. Heat. Mass Transf. 239, 126577. https://doi.org/10.1016/j.ijheatmasstransfer.2024.126577.

Nasiri, M., Hadim, H., 2024. Advances in battery thermal management: Current landscape and future directions. Renew. Sustain. Energy Rev. 200, 114611. https://doi.org/10.1016/j.rser.2024.114611.

Ouyang, D., Chung, Y., Liu, J., Bai, J., Zhou, Y., Chen, S., Wang, Z., Shu, C., 2025. Characteristics and mechanisms of as well as evaluation methods and countermeasures for thermal runaway propagation in lithium-ion batteries 108.

Ping, P., Gao, X., Kong, D., Gao, W., Feng, Z., Yang, C., Li, C., Dai, X., 2024. Experimental study on the synergistic strategy of liquid nitrogen and water mist for fire extinguishing and cooling of lithium-ion batteries. Process Saf. Environ. Prot. 188, 713–725. https://doi.org/10.1016/j.psep.2024.05.077.

Roe, C., Feng, X., White, G., Wang, Li, R., Huaibin, Rui, X., Li, C., Zhang, F., Null, V., Parkes, M., Patel, Y., Wang, Wang, Y., Hewu, Ouyang, M., Offer, G., Wu, B., 2022. Immersion cooling for lithium-ion batteries – A review. J. Power Sources 525, 231094 https://doi.org/https://doi.org/10.1016/j.jpowsour.2022.231094.

Sarkar, S., Swamy, D., Amin, T., El-halwagi, M., 2024. Safer operating areas (SOA) of cylindrical lithium-ion battery – A probabilistic approach. Process Saf. Environ. Prot. 190, 708–725. https://doi.org/10.1016/j.psep.2024.08.056.

Shabana, R., Sajid, Z., Swamy, D., Amin, T., Khan, F., 2025. Why does Ind. need Battery Saf. Manag. Syst. (BSMS)? 197.

Su, Y., Zhang, L., Zhou, Y., Geng, M., Liu, S., Chen, L., 2025. Thermal management performance of flat heat pipe in prismatic battery module. Appl. Therm. Eng. 279, 127747. https://doi.org/10.1016/j.applthermaleng.2025.127747.

Wahab, A., Najmi, A., Senobar, H., Amjady, N., Kemper, H., Khayyam, H., 2025. Immersion cooling innovations and critical hurdles in Li-ion battery cooling for future electric vehicles. Renew. Sustain. Energy Rev. 211, 115268. https://doi.org/10.1016/j.rser.2024.115268.

Wang, B., Zhou, Z., Li, L., Peng, Y., Cao, J., Yang, L., 2022. Experimental study on thermal runaway and its propagation of large format prismatic lithium-ion batteries. J. Energy Storage 55, 105550. https://doi.org/10.1016/j.est.2022.105550.

Wang, G., Gao, W., He, X., Peng, R., Zhang, Y., Dai, X., Ping, P., 2024. Numerical investigation on thermal runaway propagation and prevention in cell-to-chassis lithium-ion battery system 236. https://doi.org/10.1016/j.applthermaleng.2023.121528.

Wang, J., Li, L., Yu, K., Zhang, J., Huang, Y., Wang, Z., Wang, W., Zhao, T., Huo, S., 2025. Comprehensive investigation on the water mist inhibition efficacy towards battery thermal runaway and its smoke hazard via regulating the releasing settings. Process Saf. Environ. Prot. 204. https://doi.org/10.1016/j.psep.2025.108001.

Wang, Z., Zou, Z., Zhou, Y., Geng, X., Sun, Y., Huang, X., Hao, M., 2025. Performance comparison of battery cold plates designed using topology optimization across laminar and turbulent flow regime. Int. J. Heat. Mass Transf. 238, 126450. https://doi.org/10.1016/j.ijheatmasstransfer.2024.126450.

Weragoda, D.M., Tian, G., Burkitbayev, A., Lo, K.-H., Zhang, T., 2023. A comprehensive review on heat pipe based battery thermal management systems. Appl. Therm. Eng. 224. https://doi.org/10.1016/j.applthermaleng.2023.120070.

Xin, Z., Tang, W., Yao, W., Wu, Z., 2025. A review of thermal management of batteries with a focus on immersion cooling. Renew. Sustain. Energy Rev. 217. https://doi.org/10.1016/j.rser.2025.115751.

Yu, Y., Tian, J., Wang, J., Li, Z., Jin, K., Mei, W., Wang, Q., 2025. In-depth analysis of synergistic suppression of thermal runaway propagation in lithium-ion battery modules via combined active cooling and passive insulation. Process Saf. Environ. Prot. 197, 107026. https://doi.org/10.1016/j.psep.2025.107026.

Zhang, H., Ganesan, P., Sharma, R.K., Zubir, M.N.B.M., Badruddin, I.A., Chong, W.T., 2024. A novel overflow channel design of manifold cold plate for lithium-ion battery: A CFD study. Process Saf. Environ. Prot. 189, 648–663. https://doi.org/10.1016/j.psep.2024.06.092.

Zhang, L., Ye, F., Li, Y., Chen, M., Meng, X., Xu, J., Sun, J., Wang, Q., 2023. Experimental Study on the Efficiency of Dodecafluoro-2-Methylpentan-3-One on Suppressing Large-Scale Battery Module Fire. Fire Technol. 59, 1247–1267. https://doi.org/10.1007/s10694-022-01322-2.

Zhang, L., Jin, K., Sun, J., Wang, Q., 2024. A Review of Fire-Extinguishing Agents and Fire Suppression Strategies for Lithium-Ion Batteries Fire. Fire Technol. 60, 817–858. https://doi.org/10.1007/s10694-022-01278-3.

Zhang, L., Su, Y., Zhang, Y., Sun, P., Ye, C., Liu, Y., 2025b. Early emergency cooling for mitigating the onset of battery thermal runaway. J. Energy Storage 132, 117820. https://doi.org/10.1016/j.est.2025.117820.

Zhang, L., Liu, Y., Huang, X., Huang, X., 2025a. Intra-cell thermal runaway propagation within a cylindrical battery induced by nail penetration. Int. J. Therm. Sci. 210, 109633. https://doi.org/10.1016/j.ijthermalsci.2024.109633.

Zhang, X., Li, Z., Luo, L., Fan, Y., Du, Z., 2022. A review on thermal management of lithium-ion batteries for electric vehicles. Energy 238, 121652. https://doi.org/10.1016/j.energy.2021.121652.

Zhao, G., Wang, X., Negnevitsky, M., Zhang, H., 2021. A review of air-cooling battery thermal management systems for electric and hybrid electric vehicles. J. Power Sources 501, 230001. https://doi.org/10.1016/j.jpowsour.2021.230001.